

Pushover Analysis of I-5 RAVENNA Bridge

R. Shafiei-Tehrany, M. ElGawady*, W. Coffey
Washington State University, USA

Civil and Environmental Engineering
Pullman, WA 99163, USA

melgawady@wsu.edu

ABSTRACT: Nonlinear pushover analysis is a powerful tool for evaluating the inelastic seismic behavior of structures. This paper presents a detailed seismic analysis of a complex bridge. The I-5 Ravenna Bridge was assessed through nonlinear pushover analyses that highlights many important issues of bridges constructed on hollow core prestressed concrete piles. A three dimensional finite element analysis of the bridge have been carried out including modeling of the bridge bearings, expansions joints, and soil-structure interaction. The nonlinear response of the bridge was investigated from the first pier hinging to the inelastic equilibrium condition using three different response spectrums representing ground motions with different return periods. The effects on the seismic demand due to period lengthening and damping increase produced by structural deterioration were evaluated. The effects of three different soils on the bridge performance were investigated as well. Using dense sand increased the stiffness of the system and the ductility capacity. In addition, change the soil type has insignificant effect on the post-yielding stiffness of the bridge.

1 GENERAL INSTRUCTIONS

1.1 Introduction

The backbone of any country's economy consists of its assets of constructed facilities, such as highways, bridges. The Washington State Department of Transportation (WSDOT) developed a bridge seismic retrofit program to address state bridges that do not meet current seismic codes. Of particular interest for WSDOT are those bridges founded on pre-cast/prestressed hollow core concrete piles. The reliable detailed assessment of such bridges is vital to evaluate their seismic structural vulnerability.

For bridges under consideration to be retrofitted, structural analysis is required to evaluate seismic structural vulnerability. As an example of these bridges, the WSDOT selected the I-5 Ravenna Bridge to be assessed through detailed analysis that highlights many important issues of bridge systems constructed using hollow core prestressed piles. This paper presents the results of a nonlinear pushover analysis of a 3D finite-element (FE) model of the I-5 Ravenna Bridge. The analyses were performed to determine the anticipated response under different design-level earthquakes. Parametric studies developed using the model permitted evaluation of the effects of different assumptions about soil-structure interaction and the effective properties of structural members on the bridge seismic response.

2 BRIDGE CHARACTERISTICS AND MODELING

The I-5 Ravenna Bridge is 1310 ft (400 m) and has 19 spans. The bridge supports two lanes of traffic and it is shaped in a curve with a radius of 5787 ft (1765 m). Each of the first five bents in the North direction has six columns while each of the last three bents has seven columns. Each of the remaining bents has four columns. All columns are extended into the ground to act as pile shafts. The above ground height of the columns varies from 15 to 27 ft (4.6 to 8.2 m). The column spacing is 18 ft (5.5 m) on center for every bent. Bents have different skew angles ranging from 29 to 42° (Figure 1).

The superstructure is composed of twelve simply supported I-shaped prestressed concrete girders with a composite 5.5 in. (139.7 mm) thick cast in-place reinforced concrete deck (Figure 2). Laminated elastomeric bearing pads are used at all of the piers. The transverse resistance is provided via girder stops capable of transferring transverse forces. At each bent and at the abutments, the bridge deck is non-monolithically constructed, providing a 1 in. (25.4 mm) expansion joint.

A three-dimensional finite-element model of the bridge using SAP2000 (2007) is shown in Figure 3. The deck and girders are combined together and modeled as one line of elastic beam elements, as this

approach provides effective stiffness and mass distribution characteristics of the bridge.

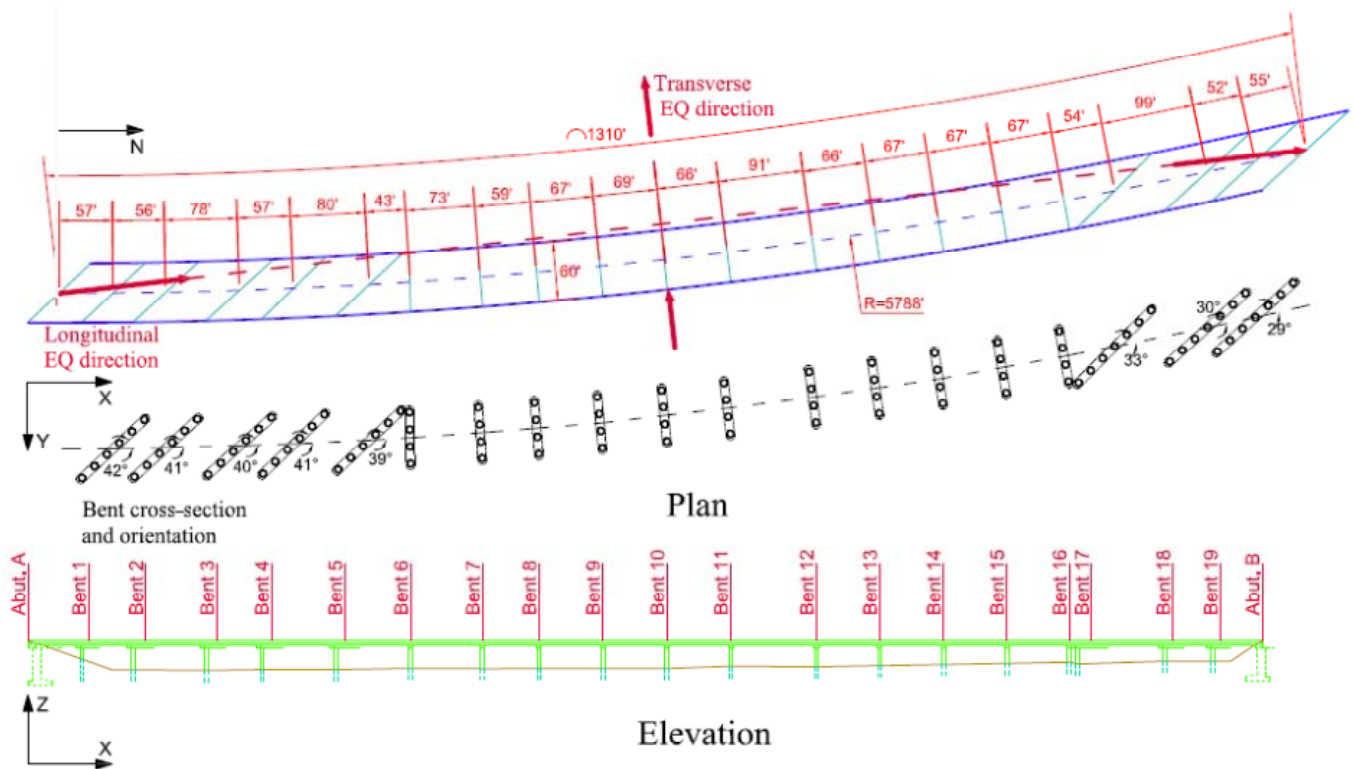


Figure 1. Plan and elevation view of the I-5 Ravenna Bridge.

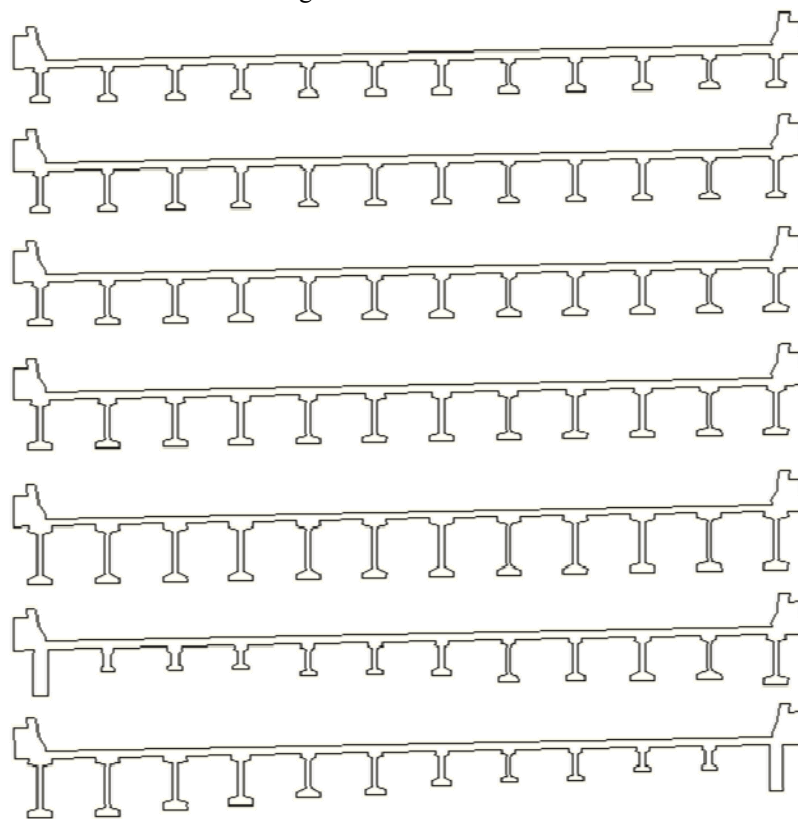


Figure 2. Superstructure cross-sections.

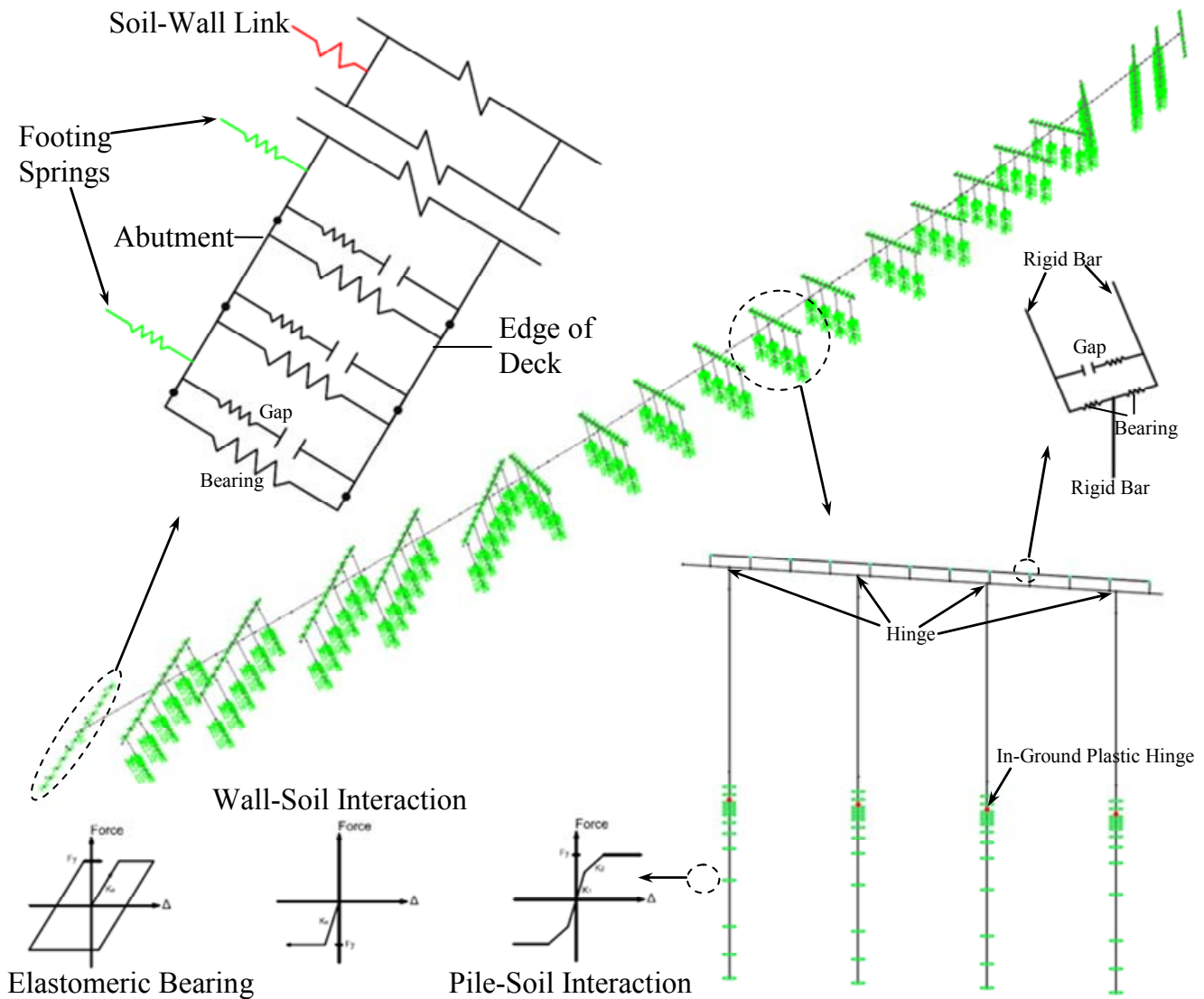


Figure 3. Three-dimensional finite-element model of the bridge using SAP2000 (2007).

The bridge superstructure itself is expected to remain essentially elastic during earthquake ground motions. Nonlinear behavior has been included for the connection between the superstructure and supporting column/abutment bents as well as the substructure.

2.1 Columns/Piles

The column cross-section is described in Figure 4. The nominal moment-curvature diagram based on different axial loads for each column section is determined using XTRACT (2002) (Figure 4). The concrete maximum compression strain was taken as 0.004 due to the absence of any significant confinement. The yield strength of the rebar steel was taken as 40 ksi (275.6 MPa). An idealized elastoplastic moment-curvature relationship was used as input to SAP2000 (2007) to describe the nonlinear behavior of the plastic hinge at the anticipated sub-grade hinge location. The column was assumed to behave linearly elastic outside the plastic hinge zone. It was

deemed sufficient to use the gross sectional moment of inertia as the effective moment of inertia for the prestressed columns (Caltrans 2008).

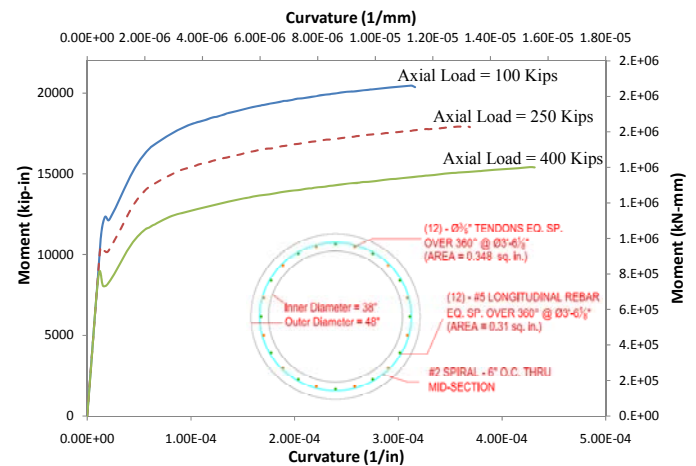


Figure 4. Moment-curvature diagrams and cross-section of columns.

Each column acts as a vertical cantilever beam because moments were released at the column-beam connection. The depth-to-maximum-moment defines the location of the in-ground plastic hinge and will influence the lateral strength and ductility capacity of the pile. The depth-to-maximum-moment, however, depends on the soil characteristics, pile diameter, and above ground column height. For the FE model, the program LPILE (2002) was used to locate the plastic hinge for varying pile aboveground heights. As the structure softens after yielding, moments are redistributed up the shaft, and the point of maximum moment (i.e., the sub-grade hinge) migrates toward the surface. Thus, depth to plastic hinge may be taken as 0.7 times the depth to maximum moment found through an elastic analysis (Budek et al. 2000). Through experimental and analytical studies, Budek et al. (1997) recommended that an in-ground plastic hinge length for a prestressed hollow pile be equal to the outer diameter of the pile.

Nonlinear springs along the pile shafts were used to model the resistance provided by the surrounding soil. L-Pile (2002) was used to compute the P-Y curves, based on selected soil characteristics. There is no confirmed data about the soil characteristics on the bridge location. Hence, the bridge was analyzed based on three different soil types, namely, loose sand, dense sand, and stiff clay with loose sand considered as the primary soil for the analysis of the bridge. The water surface level was assumed 7 ft (2.1 m) deep from the ground surface.

2.2 Abutments

The abutments on this bridge are spill-through-type with a 7 ft (2.1 m) high back wall. The back wall is connected to footings deep in the ground through columns. The first abutment has four footings and the second abutment has six footings. Based on passive earth pressure test and force deflection results from large-scale abutment testing at UC Davis (Kutter et al. 2003), the initial embankment fill stiffness is 20 kip/in/ft (11.5 kN/mm/m). The passive earth pressure reaches its maximum value when the soil reaches its ultimate strength of 5 ksf (239 kPa) after sufficiently large movements of the walls, and it remains constant for further wall movements (Caltrans 2008b). Nonlinear plastic links were developed for the back wall soil interaction. Linear springs were calculated for the footings by following the FEMA 356 (2000) procedure, based on the geometric characteristics of the abutment footing. The stiffness of the footings was activated for the movement of the abutments in all six global degree of freedom. The abutments provide resistance only when the ini-

tial gap of 1 inch between the abutments and the superstructure is closed.

2.3 Gap Elements

The gap element of SAP2000 (2007) was utilized to account for the possibility of pounding when the longitudinal deformations close the gaps between spans as well as the gaps at the abutments. The gap element was set as a "compression-only" connection such that the element did not apply any resistance before the closure of the gap. When the gap between the deck and abutment closed, pounding occurred. Infinite stiffness of the gap element can be assumed at the contact location (Caltrans 2008a).

2.4 Bearings

The longitudinal stiffness of the bearing pads was calculated as follows:

$$k = \frac{GA}{h} \quad (1)$$

where G is the shear modulus, A is the cross-sectional area, and h is the bearing height. The other stiffness of the bearing pads were set relatively high to model the resistance of the girder stops in the transverse and rotational degrees of freedom of the bridge.

The lateral shear capacity of elastomeric bearing pads is controlled by either the dynamic friction capacity between the pad and the bearing seat or the shear strain capacity of the pad. Caltrans (2008a) recommended using a dynamic coefficient of friction between concrete and neoprene of 0.40. The maximum shear strain resisted by elastomeric pads prior to failure is estimated at +/-150% (Caltrans 2008a).

3 CAPACITY SPECTRUM METHOD FOR PUSHOVER ANALYSIS

Pushover analysis is composed of three primary elements (ATC 1996): (1) the step-by-step development of the capacity curve of the bridge. This is a plot of the lateral force applied to the bridge at various increments of loading versus the lateral displacement of the bridge under that applied lateral force; (2) determine the displacement demand on the bridge using nonlinear demand spectra; and (3) identification of the performance point, i.e., expected displacement during the Design Level Earthquake (DLE) and the subsequent check to ensure that this is acceptable structure performance. To determine the performance point, the capacity and displacement demand curves should be plotted in the Acceleration-Displacement Response Spectra (ADRS) domain in which spectral acceleration is drawn against spectral displacement.

The nonlinear displacement demand spectra is derived from the elastic 5% damped response design spectrum after applying spectral reduction factors. The factors are function of the effective damping which depends on the performance point among other factors as explained in the next paragraph. Hence, determination of the performance point could be a trial and error procedure. Instead, the performance point can be determined by overlaying the capacity spectrum onto a single displacement demand spectrum with variable damping (ATC 1996). The single displacement demand spectrum curve is constructed by doing the following for each point on the ADRS pushover curve: (1) a radial line through the point on the ADRS pushover curve is drawn which a constant period; (2) the damping associated with the point on the curve is calculated using equation 2; and (3) the demand spectrum is constructed, plotting it for the same damping level as associated with the point on the pushover curve. The intersection point of the radial line and the associated demand spectrum represents a point on the single demand spectrum curve. The intersection of the single demand spectrum curve and the capacity curve represents the performance point. This procedure is similar to Procedure B in chapter 8 of ATC-40 (10), except that it does not make the simplifying assumption that the yielding stiffness remains constant.

The equivalent viscous damping ration of the inelastic system, ζ_{eq} , is obtained by equating the energy dissipated in one cycle of motion for the inelastic system and the equivalent linear system. The equivalent viscous damping ratio can be determined as follows (Chopra and Goel 1999):

$$\zeta_{eq} = \frac{2}{\pi} \frac{(\mu-1)(1-\alpha)}{\mu(1+\alpha\mu-\alpha)} \quad (2)$$

where μ is the displacement ductility of the structure and α is the ratio of post to pre-yielding stiffness. The equivalent viscous damping may be modified by a damping modification factor, κ , which accounts for the variation of the actual hysteresis loops from the idealized parallelogram associated with bilinear hysteresis. In this study, the value of κ was taken equal to 2/3 corresponding to Structure Type B in ATC 40 (10). This κ value assumed that the bridge has an average seismic resistance system.

The equivalent natural period, T_{eq} , of the bilinear system is based on the secant stiffness at a given displacement level and is given by:

$$T_{eq} = T_n \sqrt{\frac{\mu}{1+\alpha\mu-\alpha}} + 5\% \quad (3)$$

,where T_n is the natural period associated with elastic behavior.

4 SEISMIC PERFORMANCE OF I-5 RAVENNA BRIDGE

A pushover analysis first requires a dynamic analysis, as lateral accelerations are applied in proportion to the fundamental modal shape. For loose sand, and by neglecting second-order effects, the longest-periods in the longitudinal and transverse directions were 1.28, and 1.24 seconds, respectively. The mode for the longest period in the longitudinal direction excited 52.16% of the system mass in the longitudinal direction and 0% in the transverse direction. The mode for the longest period in the transverse direction excited 54.8% of the system mass in the transverse direction and 0% in the longitudinal direction.

Separate pushover analysis was performed in the longitudinal and transverse directions of the bridge. Since the bridge is not symmetric, analysis was carried out for both positive and negative transverse directions. Three elastic design response spectra, for soil class C, corresponding to 100, 1000, and 2475-year return period, were developed for Seattle area (USGS 2002). The lateral acceleration thus obtained was applied to all model nodes in proportion to the respective longest-period modal shapes. Structure displacements were read at the super structure mass centroid.

The analysis of the lateral capacity of the bridge ended when the first plastic hinge reached its rotation capacity. This condition is shown in Figures 5 and 6 for the transverse and longitudinal directions, respectively. In these figures plastic hinges are represented by dots, and the hinging sequence is numbered. The piers that reached their ultimate rotational capacity were circled. The curved shape of the bridge provides a slightly higher stiffness in the positive transverse direction than in the negative transverse direction, which resulted in a more severe hinge formation in the positive direction. The piles of the center bents experienced the first yielding and ultimately failed for both longitudinal and transverse pushover analyses.

The capacity curves for the pushover analyses are shown in Figure 7. The dots describe the main phases of plastic hinging according to the hinge numeration of Figures 5 and 6. The transverse capacity curves have very similar characteristics. The ULS displacement and the first yielding displacement exhibited less than 3% difference between the two transverse directions capacity curves. Based on these results, it was decided to continue the analysis considering only one transverse direction.

Figure 7 shows that the initial stiffness of the transverse direction is 13% slightly higher than the initial stiffness of the longitudinal direction. In addition, post yielding stiffness in the longitudinal direction was higher than the transverse directions. This

occurred as 54% and 64% of the piles in the transverse and longitudinal directions, respectively, respond elastically until the bridge reached its ULS. The displacement capacity for both directions was approximately equal. However, the transverse direction reached this displacement at strength 10% higher than the strength of the longitudinal direction.

ζ_{eq} and T_{eq} were calculated using Equations 2 and 3, respectively, for the longitudinal and transverse directions (Figures 8 and 9). As shown in the figures, both ζ_{eq} and T_{eq} increased with increased

bridge lateral displacement. At ULS (Figure 8), the transverse direction reached ζ_{eff} of 8.57% while the longitudinal direction reached only 7.43%. At ULS (Figure 9), the effective fundamental period increased by approximately 12.75% and 9.56% in the transverse and longitudinal directions, respectively. ζ_{eff} and T_{eq} increased in the transverse direction more than the longitudinal direction due to the larger reduction in the system stiffness resulting from structural deterioration and hinge formation.

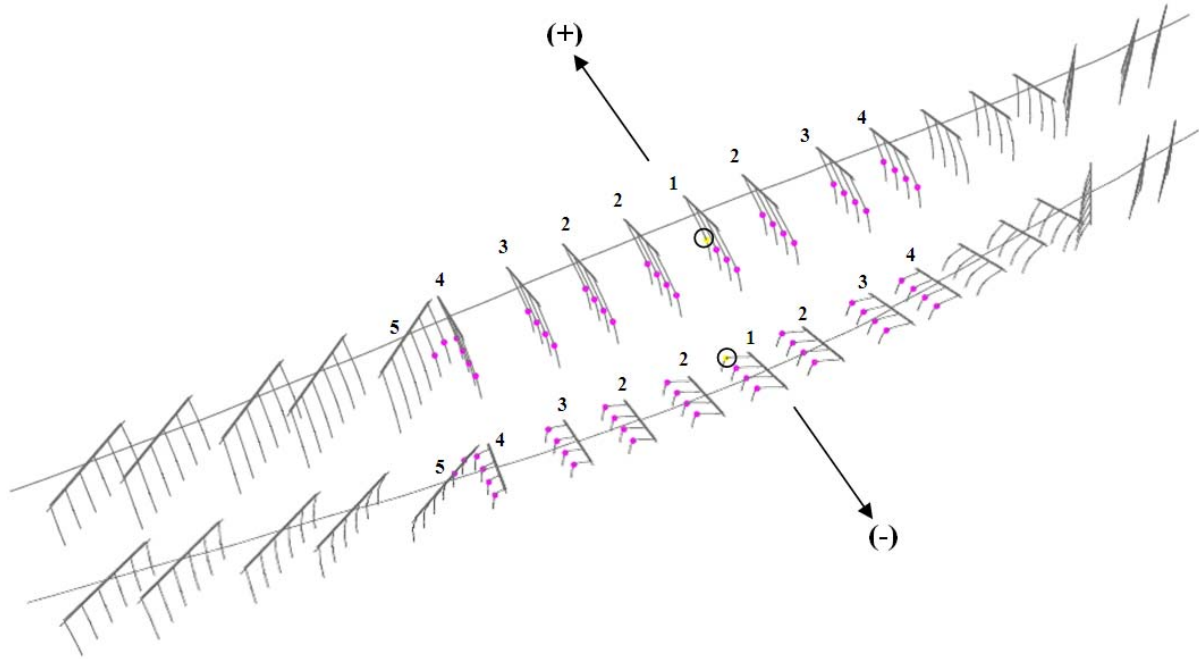


Figure 5. Hinging sequence up to transverse ultimate limit state condition.

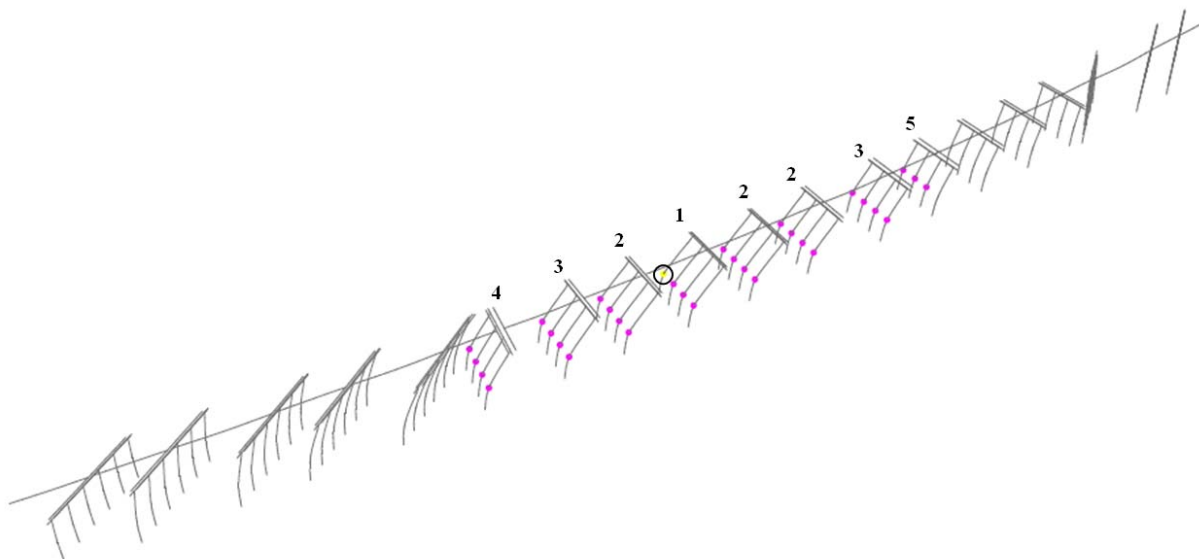


Figure 6. Hinging sequence up to longitudinal ultimate limit state condition.

As mentioned, three variable-damping spectra corresponding to 100 (Earthquake 1 or EQ1), 1000 (EQ2), and 2475-year (EQ3) return period were used

for assessment of the bridge. Table 1, Figures 10, and 11 present the displacements corresponding to the performance points for each spectrum as well as

the displacement corresponding to the 1st yield, ULS, and the displacement ductility capacity. In addition, the displacement ductility demand for each earthquake is presented in Table 1. Finally, the effects of the damping modification factor, κ , on the spectral displacement are shown in Figures 10 and 11. Where type A corresponding to well-designed structures and type C corresponding to existing structures having deficient seismic details.

As shown in the figures and table, the displacement corresponding to the performance points in the longitudinal direction under the 2475, 1000, and 100-year return period were 74, 60, and 45% of the ULS displacement, respectively. The displacement demand in the transverse directions was more critical. The displacement corresponding to the performance points in the transverse directions under the 2475, 1000, and 100-year return periods were 88, 67, and 23% of the ULS displacement, respectively.

The displacement ductility demand during a given earthquake level is described by the ratio of the lateral displacement at the performance point during this earthquake to the first-yield displacement.

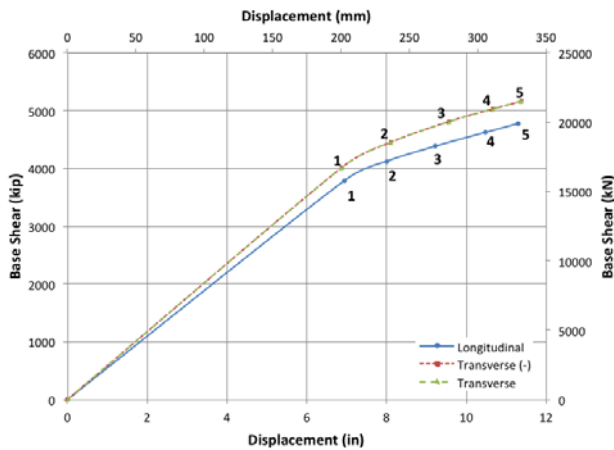


Figure 7. Capacity curves for longitudinal and transverse directions.

Table 1. Summary of the nonlinear static analyses with different soil types

	Model Analysis		System Capacity			Performance Points			Demand Ductility		
	Period (sec)	MPMR (%)	1 st Yield (in.)	ULS (in.)	Ductility	EQ1 (in.)	EQ2 (in.)	EQ3 (in.)	EQ1 (in.)	EQ2 (in.)	EQ3 (in.)
Longitudinal											
Loose Sand	1.37	52.18	6.92	11.19	1.62	5.02	6.68	8.24	0.73	0.97	1.19
Dense Sand	1.04	39.92	3.58	7.61	2.13	2.52	3.08	3.77	0.36	0.45	0.54
Stiff Clay	1.02	44.63	6.65	11.07	1.66	3.33	4.46	5.86	0.48	0.64	0.85
Transverse											
Loose Sand	1.32	54.87	6.96	11.39	1.64	7.04	8.65	10.76	1.02	1.25	1.55
Dense Sand	0.94	56.22	3.45	7.39	2.14	4.35	5.50	6.84	0.63	0.79	0.99
Stiff Clay	0.97	48.20	6.75	11.19	1.66	5.34	7.13	9.42	0.77	1.03	1.36

MPMR is the modal participation mass ratio

1st yield is the considered displacement at which the first column starts yielding

Table 1 presents both the first yield and the ductility demand for the three different earthquakes. The 100-year return period lied approximately in the elastic region of the capacity-demand spectra for both longitudinal and transverse directions, and thus its ductility demand was smaller than or equal to approximately 1. The ductility demand in the longitudinal direction was 0.97 and 1.19 for the 1000-year and 2475-year return period response, respectively.

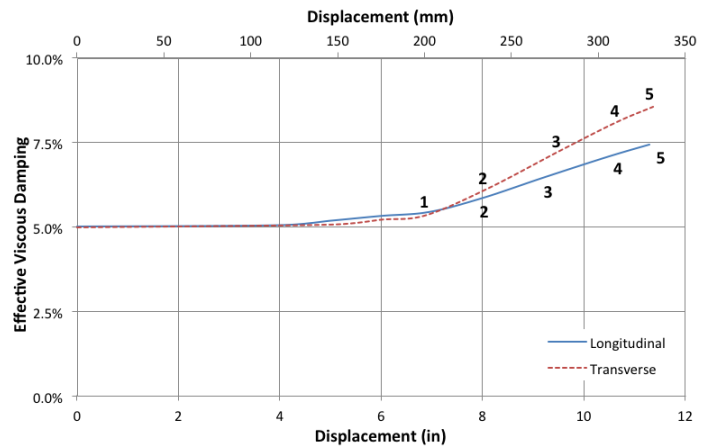


Figure 8. Yielding increase in equivalent viscous damping.

The ductility demand in the transverse direction was 1.25 and 1.55 for the 1000-year and 2475-year return period, respectively. Finally, as shown in the figures, the damping modification factor, κ , has limited effects on the displacements at the performance points. The effect of κ is higher for 2475-year return period earthquake. In creasing the value of κ (i.e. moving from type C to type A) reduced the spectral displacements at the different performance points by an average of 10%.

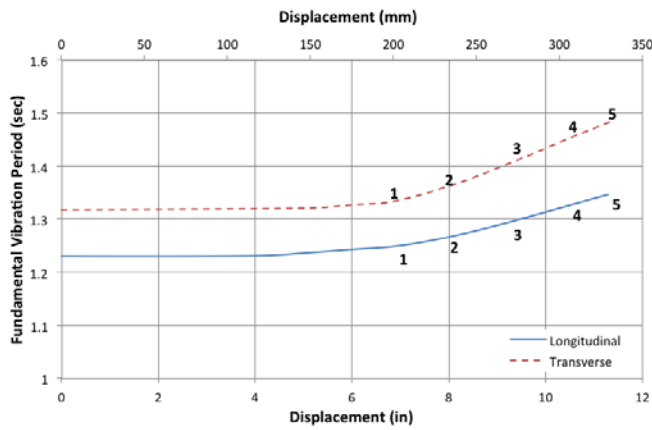


Figure 9. Influence of lateral displacement on the natural period.

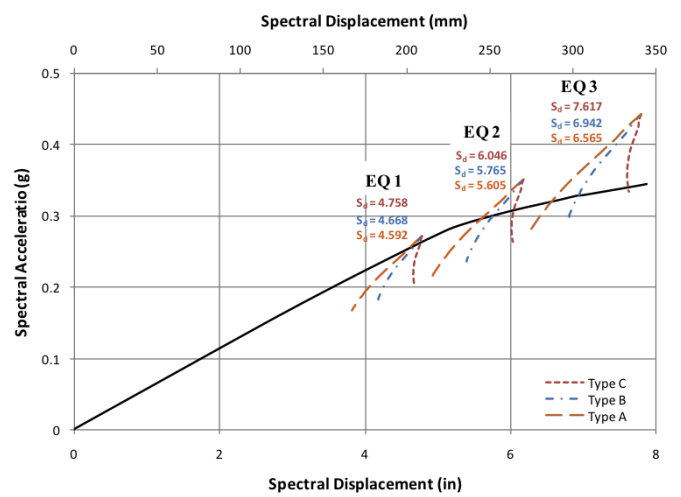


Figure 11. Capacity-demand comparisons for longitudinal pushover.

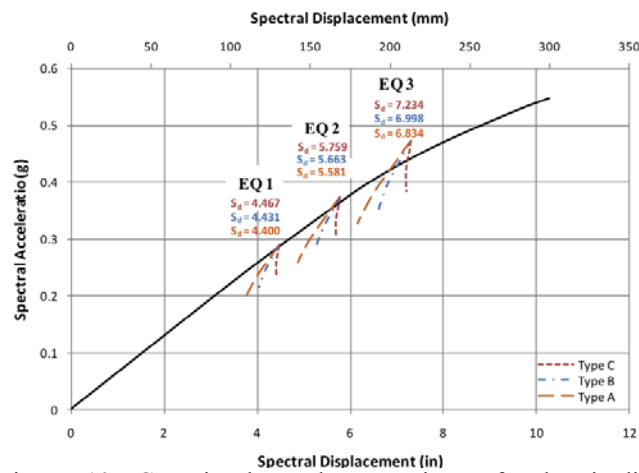


Figure 10. Capacity-demand comparisons for longitudinal pushover.

5 EFFECTS OF SOIL PROPERTIES ON BRIDGE SEISMIC PERFORMANCE

The I-5 Ravenna Bridge is founded on layers of sandy gravel and sandy clay with varying thickness. The dynamic soil-structure interaction (SSI) was initially modeled based on the assumption that a loose sand soil condition would best capture the actual soil condition. Because of the influence of the inherent uncertainties in boundary conditions on the expected displacements of the structure, the pile and abutment springs were also modeled based on other two soil types: dense sand and stiff clay. Sub-grade plastic hinge locations were modified using L-pile (2) for each soil type. The capacity curve for the different soil types is shown in Figures 12 and 13 for longitudinal and transverse directions, respectively. Also, the different displacements and ductility demands for the different soil types are presented in Table 1.

For both directions, the post yield stiffness of the structure is similar for all three-soil conditions. This may be interpreted, as the pile's performance was independent of the confining soil after hinge formation had taken place.

Changing the soil type from loose sand to stiff clay or dense sand increased the initial stiffness in the longitudinal direction by 50 and 52%, respectively. In addition, the longitudinal ULS displacement reduced from 11.19 in. (284 mm) for loose sand condition to 11.07 and 7.61 in. (281 and 193 mm) for stiff clay and dense sand conditions, respectively (table 1). In the transverse direction, changing the soil type from loose sand to stiff clay or dense sand increased the initial stiffness by 58 and 120%, respectively. Also, the transverse ULS displacement reduced from 11.39 in. (289 mm) for loose sand condition to 11.19 and 7.39 in. (284 and 188 mm) for stiff clay and dense sand condition, respectively (table 1). Also, Table 1 presents effects of the soil type on the performance point corresponding to the three different spectra. As shown in the table going from loose sand to dense sand decreased the displacements by an average of 45%. The decrease was more pronounced for the 2475-year return period earthquake. As a conclusion, different mechanical properties of pile and abutment springs resulted in significant variations in the expected inelastic displacements.

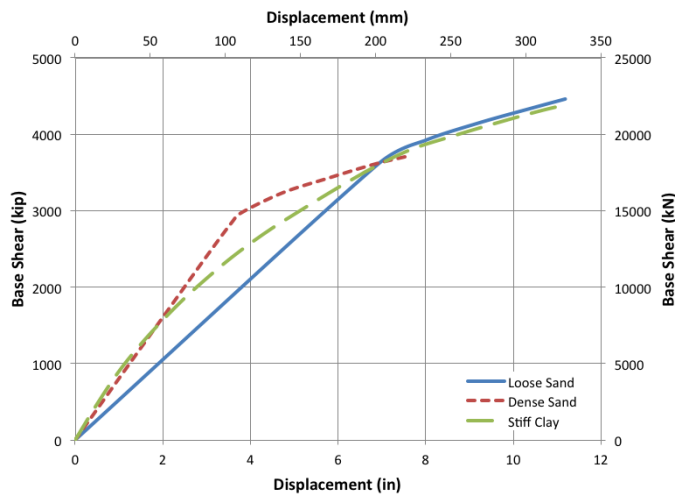


Figure 12. Effects of soil type on the bridge capacity in the longitudinal direction.

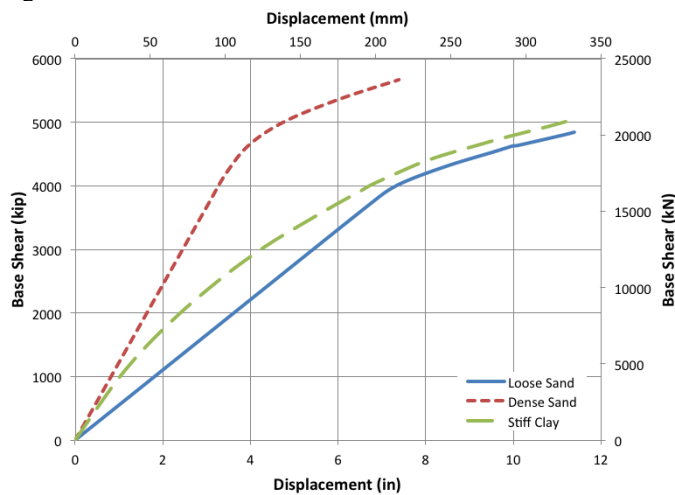


Figure 13. Effects of soil type on the bridge capacity in the transverse direction.

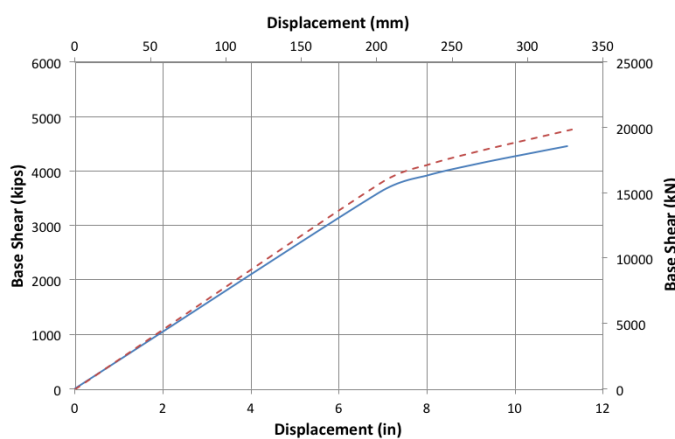


Figure 14. Longitudinal capacity curve with (continuous line) and without P-delta effects.

6 SECOND-ORDER EFFECTS OF GEOMETRIC NONLINEARITY (P-DELTA)

In this section, the influence of the P-delta effect on the performance of the bridge is investigated. Figures 14 and 15 present comparisons between the ca-

capacity curves with and without P-delta effects for the longitudinal and transverse directions, respectively. As shown in the figure, the geometric nonlinearity resulted in a decrease in the initial stiffness by 10.5% and 11.2% in the longitudinal and transverse directions. These reductions resulted in slight increase in the fundamental periods of the undamaged structure, from 1.366 to 1.395 seconds (+2.1%) for longitudinal, and 1.322 to 1.350 seconds (+2.1%) for transverse. The strength capacity decreased in both directions by approximately 6.5%.

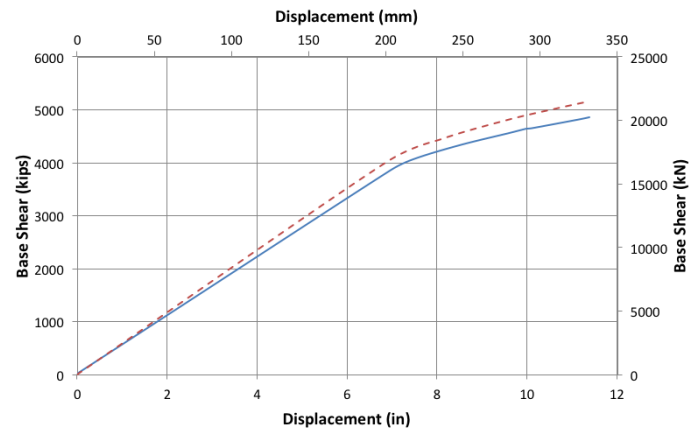


Figure 15. Transverse capacity curve with (continuous line) and without P-delta effects.

7 CONCLUSION

Nonlinear pushover analysis is a powerful tool for evaluating the inelastic seismic behavior of structures. Based on the results of the hinge formation sequence, the center bents should be targeted first for retrofitting since they yielded first. Bent #10 in particular contained the column that failed first in all pushover analyses. The parametric study with different soils showed that the initial stiffness of the structure is significantly affected by the soil type. However, the post-yielding stiffness was essentially the same regardless of the soil characteristics. The bridge displacement capacity decreased in average by 43% going from loose sand to dense sand. However, displacement demand decreased when replacing loose sand by dense sand. Based on the ductility demand to the ductility capacity of the bridge it seems that the loose sand represented the worst-case scenario. Inclusion of the P-delta effects slightly deteriorates the bridge performance.

8 ACKNOWLEDGEMENTS

Funding for this research was provided by the Washington State Department of Transportation (WSDOT). Their assistance is greatly appreciated.

REFERENCES

- Applied Technology Council (ATC). (1996). "Seismic Evaluation and Retrofit of Concrete Bridges." *ATC-40*, Redwood City, California.
- Budek, A. M., Priestley, M. J. N., and Benzoni, G. (2000). "Inelastic seismic response of bridge drilled-shaft RC pile/columns." *J. Struct. Eng.*, 126(4), 510–517.
- Budek, Andrew M., Gianmario Benzoni, and M. J. Nigel Priestley. *Experimental investigation of ductility of in-ground hinges in solid and hollow prestressed piles*. La Jolla, Calif.: Structural Systems Research, Univ. of California, San Diego, 1997. 108 p. (SSRP-97/17).
- Caltrans (2008). *Seismic Design Criteria 1.4*. California Department of Transportation
- Caltrans. *Seismic Design Criteria 1.4*. (2008). California Department of Transportation.
- Chopra AK, Goel RK. Capacity-demand-diagram-methods for estimation seismic deformation of inelastic structures: SDF Systems. Report No. PEER-1999/02. Berkeley (CA): Pacific Earthquake Engineering Research Center, University of California at Berkeley; 1999.
- Federal Emergency Management Agency, (2000). *Prestandard and Commentary for the Seismic Rehabilitation of Buildings (FEMA 356)*. Washington, D.C.
- Kutter, B. L., Martin, G., Hutchinson, T., Harden, C., Gajan, S., and Phalen, J. (2003). "Study of Modeling of Nonlinear Cyclic Load-Deformation Behavior of Shallow Foundations." Status report, PEER workshop, March, 5, 2003, Berkeley, California.
- L-Pile Plus 4, (2002) ENSOFT, INC.'s.
- Priestley, M. J. N., Seible, F., and Calvi, G. M. (1996). *Seismic design and retrofitting of bridges*, Wiley, New York.
- SAP2000 11.0.0 Structural Analysis Program (2007). Computer and Structures, Inc. Berkeley, California.
- U.S. Geological Survey (USGS). (2002). "Seismic hazard maps for the conterminous U.S. for 2002." *USGS Earthquake Hazards Program*, <<http://earthquake.usgs.gov>> (July 20, 2008).
- XTRACT v.2.6.2 Educational, Cross Section Analysis Program (2002), Imbsen and Associates, Inc., Sacramento, California.